Applied Physics Letters

Analytical model for light modulating impedance spectroscopy (LIMIS) in all-solid-state p-n junction solar cells at open-circuit

Cite as: Appl. Phys. Lett. **116**, 013901 (2020); https://doi.org/10.1063/1.5139571
Submitted: 21 November 2019 . Accepted: 18 December 2019 . Published Online: 02 January 2020

Osbel Almora, Daniel Miravet, Gebhard J. Matt, Germà Garcia-Belmonte, and Christoph J. Brabec

Applied Physics Letters ARTICLE scitation.org/journal/apl

Analytical model for light modulating impedance spectroscopy (LIMIS) in all-solid-state p-n junction solar cells at open-circuit

Cite as: Appl. Phys. Lett. **116**, 013901 (2020); doi: 10.1063/1.5139571
Submitted: 21 November 2019 · Accepted: 18 December 2019 ·
Published Online: 2 January 2020

Osbel Almora,[1,2,3,a)] Daniel Miravet,[4] Gebhard J. Matt,[1] Germà Garcia-Belmonte,[3] and Christoph J. Brabec[1]

AFFILIATIONS

[1]Institute of Materials for Electronics and Energy Technology (i-MEET), Friedrich-Alexander-Universität Erlangen-Nürnberg, 91058 Erlangen, Germany
[2]Erlangen Graduate School in Advanced Optical Technologies (SAOT), Friedrich-Alexander-Universität Erlangen-Nürnberg, 91052 Erlangen, Germany
[3]Institute of Advanced Materials (INAM), Universitat Jaume I, 12006 Castelló, Spain
[4]Centro Atómico Bariloche, CNEA, CONICET, 8400 Río Negro, Argentina

[a)]**Author to whom correspondence should be addressed:** osbel.almora@fau.de

ABSTRACT

Potentiostatic impedance spectroscopy (IS) is a well-known tool for characterization of materials and electronic devices. It can be complemented by numerical simulation strategies relying on drift-diffusion equations without any equivalent circuit-based assumptions. This implies the time-dependent solutions of the transport equations under small perturbation of the external bias applied as a boundary condition at the electrodes. However, in the case of photosensitive devices, a small light perturbation modulates the generation rate along the absorber bulk. This work then approaches a set of analytical solutions for the signals of IS and intensity modulated photocurrent and photovoltage spectroscopies, intensity modulated photocurrent spectroscopy (IMPS) and intensity modulated photovoltage spectroscopy (IMVS), respectively, from one-sided p-n junction solar cells at the open-circuit. Subsequently, a photoimpedance signal named "light intensity modulated impedance spectroscopy" (LIMIS = IMVS/IMPS) is analytically simulated, and its difference with respect to IS suggests a correlation with the surface charge carrier recombination velocity. This is an illustrative result and the starting point for future more realistic numerical simulations.

The concept of impedance as a transfer function in the form of a ratio between two complex magnitudes has been widely tackled, since its introduction by Heaviside.[1] The most typical application comprises the study of the electrical current response to small voltage perturbation, as in standard potentiostatic impedance spectroscopy (IS) where the impedance itself Z has units of Ohms.[2] IS is a well-known and established characterization technique for the evaluation of the resistive, capacitive, and inductive features of materials and electronic devices. Particularly, on photovoltaic solar cells, IS typically informs on the recombination modes,[3] the doping densities,[4,5] deep defect levels,[6] and the density of states.[7]

One of the most common practices in solar cell characterization is to measure potentiostatic IS at an open-circuit (OC) condition under a series of steady-state direct current ("dc") mode illumination intensities. By this way, assisted by numerical circuit theory calculations, the recombination resistance R_{rec}, chemical capacitance C_μ, and characteristic lifetimes τ can be evaluated, among other parameters.[3,8,9] Also, drift-diffusion numerical calculations have been reported solving the time-dependent continuity and Poisson's equations under small perturbation of the bias boundary condition at the electrodes.[10–13]

Alternatively, in photosensitive samples, the current or voltage responses to small light intensity perturbations can also be studied, which are the cases of intensity modulated photocurrent spectroscopy (IMPS)[14–25] and intensity modulated photovoltage spectroscopy (IMVS),[20,21,26–28] respectively. IMVS and IMPS individually characterize the current and voltage responsivities Ψ_J and Ψ_V, respectively. Similar to IS, we can take the ratio IMVS/IMPS to define light intensity modulated impedance spectroscopy (LIMIS). This relation was first introduced by Song and Macdonald[29] who measured the spectra on n-Si in KOH solution, validating the transfer function by Kramers–Kronig transformation. Later, Halme[30] applied the concept to dye sensitized solar cells, concluding the approximate equivalence between IS and LIMIS. Furthermore, in

our simultaneous and complementary study,[8] we measured LIMIS in all-solid-state silicon, organic, and perovskite solar cells and numerically simulated LIMIS spectra with the circuit-based approach, showing qualitative and quantitative differences between IS and LIMIS. These differences were shown to imply corrections to the evaluation of the carrier lifetimes and the empirical form of the Shockley equation.

Understanding the difference between the transfer functions resulting from IS and LIMIS demands a model able to reproduce and explain the experimental patterns. Thus, the accurate solving of the drift-diffusion equations would possibly be the best resource, requiring the use of numerical methods to reproduce the frequency-dependent signals around the OC steady-state under dc illumination. In the case of LIMIS, or individually IMPS and IMVS, the complete development of the time dependent numerical solutions is still in early phases,[10] and such a task is beyond the scope of this paper. Instead, the focus is set here on the analytical solution for the particular case of one-sided abrupt p-n junction thin film solar cells. This model is of special interest regarding the moderately doped p-type base in contact with a highly doped n-type emitter, which is the usual case for p-n$^+$ silicon solar cells.

In this article, we further analyze the LIMIS concept at OC and solve the drift-diffusion equations in an analytical approximation for the one-sided p-n junction solar cells that suggest a correlation between the surface recombination velocity and the difference between IS and LIMIS. These analytical results complement the typical equivalent circuit-based approach studies and set a starting point for future numerical drift-diffusion simulations.

Introducing the formalism, with the notation in Table S1, the supplementary material provides a helpful step-by-step description of the following deductions. Additionally, in Sec. S1.2., the continuity equation (S9) is shown with the drift and diffusion terms, the Poisson equation, the drift-diffusion currents, and the boundary conditions (S10) for the electrostatic potential φ and the current in the assumption of Ohmic contacts for the solution of the numerical problem. The numerical problem is beyond the scope of this work, and so we proceed with our analytical deductions.

Now, let us first consider a sinusoidal $\tilde{V}(t)$ small perturbation applied to a generic sample at steady-state voltage $\overline{V}$. Then, the current response around the steady-state value $\overline{J}(\overline{V})$ may be ϕ phase shifted as $\tilde{J} = |\tilde{J}|\exp[-i\phi]$, resulting in the impedance as

$$Z(\omega) = \frac{\tilde{V}(t)}{\tilde{J}(t)} = \frac{|\tilde{V}|}{|\tilde{J}|}\exp[i\phi], \tag{1}$$

with i being the imaginary number. Now, instead, the perturbation can be done by a light source in photosensitive samples. Then, a small perturbation $\tilde{P}_{in}(t) = |\tilde{P}_{in}|\exp[i\,\omega t]$ can be added to the given dc incident light power density $\overline{P}_{in}$. Upon this perturbation, both current and voltage signals can be recorded, and so the current responsivity transfer function is

$$\Psi_J(\omega) = \frac{\tilde{J}}{\tilde{P}_{in}} = \frac{|\tilde{J}|}{|\tilde{P}_{in}|}\exp\left[i\phi_J\right], \tag{2}$$

and, at OC ($J = 0$), the modulated photovoltage signal $\tilde{V}_{oc} = |\tilde{V}_{oc}|\exp[i\phi_V]$ gives the voltage responsivity transfer function as

$$\Psi_V(\omega) = \frac{\tilde{V}_{oc}}{\tilde{P}_{in}} = \frac{|\tilde{V}_{oc}|}{|\tilde{P}_{in}|}\exp[i\phi_V]. \tag{3}$$

Equations (2) and (3) define by themselves IMPS and IMVS, respectively. These techniques have been earlier introduced,[14–17,23,27,31] and there have been recent studies on photovoltaic solar cells.[21,22,24,28,32] Now, as discussed before,[8] it can be advantageous to combine IMPS and IMVS in addition to individually analyze them. Therefore, we obtain light intensity modulated impedance spectroscopy (LIMIS) as

$$Z_\Psi(\omega) = \frac{\Psi_V}{\Psi_J} = \frac{|\tilde{V}_{oc}|}{|\tilde{J}|}e^{i\left(\phi_V - \phi_J\right)} = |Z_\Psi|e^{i\,\phi_\Psi}. \tag{4}$$

From the drift-diffusion equations in the perfect selectivity approximation and the above definitions, we can deduct the alternating current ("ac") mode for the modulated currents[2]

$$\tilde{J} \cong q\int_0^L \left[\tilde{G} - \tilde{n}\left(\frac{1}{\tau} + 2\beta\overline{n}_0 + i\omega\right)\right]dx. \tag{5}$$

Also, parting from the typical V_{oc} definition and using the McLaurin series, the modulated photovoltage can be found as[27]

$$\tilde{V}_{oc} \cong 2\frac{k_BT}{q}\frac{\tilde{n}}{\overline{n}_0}, \tag{6}$$

where q is the elementary charge, k_BT is the thermal energy, L is the effective distance between electrodes or effective current integration length, $\tilde{G}$ is the ac generation rate, τ is the nonradiative surface/Shockley-Read-Hall (SRH) recombination lifetime, β is the second order direct free carrier recombination coefficient (typically, radiative recombination coefficient), $\overline{n}$ is the steady-state overequilibrium concentration (under dc bias and/or illumination), and $\tilde{n}$ is the complex ac amplitude response to $\tilde{V}$ or $\tilde{P}_{in}$, which includes the phase shift ϕ_n, i.e., $\tilde{n} = |\tilde{n}|\exp[i\phi_n]$.

Accordingly, the task here is to solve the transport equations to obtain $\overline{n}$ and $\tilde{n}$ for the dc and ac solutions and then substitute in (1)–(6). Here, we highlight that IS and LIMIS are different regarding "where" the perturbation is applied. In IS, $\tilde{V}$ directly affects the φ boundary condition, which defines the electric field ξ after Poisson's equation. Later, its effect will be particularly related to recombination and its influence in the space charge region in the continuity equation.

On the other hand, the perturbed term in LIMIS is directly affecting the continuity equation via the generation rate G along the effective absorber layer bulk section. Assuming a light intensity independent incident light spectrum, G can be expressed in dc and ac real terms as

$$G(t) = \overline{G} + \tilde{G}\,e^{i\omega t} = \frac{\Psi_{sc}}{qL}\left(\overline{P}_{in} + \tilde{P}_{in}\,e^{i\omega t}\right), \tag{7}$$

where L is the effective absorber layer thickness where the current is integrated and Ψ_{sc} is the photocurrent responsivity at the short-circuit that depends on the incident light spectrum, the absorption coefficient, and the geometry of the absorbing materials. Note that $\tilde{G} = |\tilde{G}|$ and $\tilde{P}_{in} = |\tilde{P}_{in}|$ are the perturbation, and similar to $\tilde{V}$, we will omit the modulus notation in the next. Also, note that only in thin film devices, (7) can be properly approached to a space independent constant G; otherwise, the Beer–Lambert law should be considered, resulting in a $G(x, t)$ dependency. For example, the use of space constant G gives a rough approximation in p-n$^+$ silicon solar cells, which are of special interest for our model. Subsequently, the inclusion of $\tilde{G}$ in the continuity equation defines the diffusion currents out of the space charge

region or in situations dominated by low field effects. This can be particularly significant for the current boundary condition.

Keeping this in mind, the analytical solution of the charge carrier concentrations around OC under $\tilde{V}$ and $\tilde{G}$ perturbations, for IS and LIMIS, respectively, can be found by structuring the solutions in the form

$$n(t) = \overline{n}_0 + \tilde{n}\exp[i\omega t], \tag{8}$$

where $\overline{n}_0 = \overline{n} + n_0$, with n_0 being the dark equilibrium concentration. In p-n$^+$ junction devices, expression (8) indicates electron density in the p-doped base and, analogously, it would be the hole concentration in the n-side of p$^+$-n junction cells.

The current boundary condition can be taken as $D\,d\tilde{n}/dx \cong S_r\tilde{n}$ in the form of Ohmic contact selectivity with diffusion coefficient D (negligible drift current), where minority carriers recombine with surface recombination velocity S_r. No significant difference was considered between IS and LIMIS regarding the S_r constraint.

On the other hand, the potential boundary condition was chosen as the depletion approximation, expressing how the different measuring ways ideally affect the charge carrier distributions and hence the energy diagram. This is summarized in Fig. 1. For IS, the $\tilde{V}$ small perturbation changes the dc depletion region width $\overline{w}$ and ac amount $\tilde{w}$ and creates small charge carrier gradients around the steady-state OC distribution. For the IMVS, the $\tilde{G}$ small perturbation also changes $\tilde{w}$ around $\overline{w}$, but without gradients, and so the charge profile is flat all the time. Finally, for IMPS, no change on $\overline{w}$ is assumed and the opposite gradient of the energy bands takes place.

Accordingly, the solution of the transport equations with the above boundary conditions approaches the impedance from IS at OC as

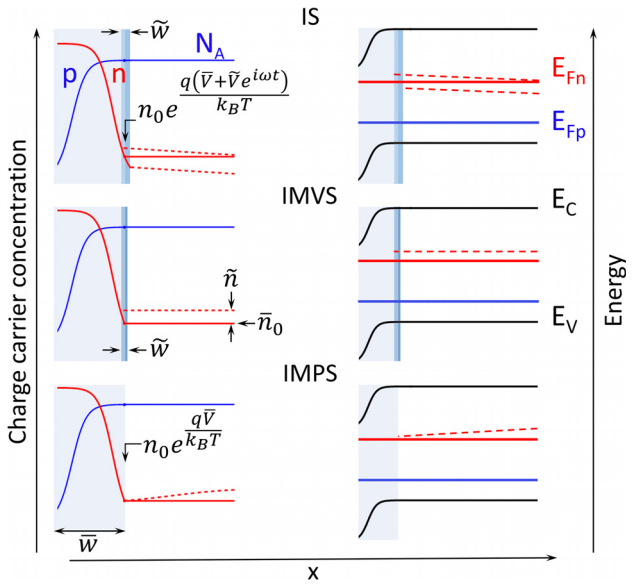

FIG. 1. Voltage boundary condition in the depletion approximation as illustrated by the charge carrier (left) and energy diagram (right) for the perturbations around the open-circuit for IS, IMVS, and IMPS, as indicated. The dashed lines represent the perturbed quantities. E_C and E_V are the minima and maxima of the conduction and valence bands, respectively.

$$Z(\omega) \cong \frac{2k_BT}{q^2\overline{L}_d\overline{G}}\frac{1}{\tilde{\gamma}\sqrt{1+i\dfrac{\omega}{\omega_0}}}, \tag{9}$$

where $\overline{L}_d = \sqrt{D/\omega_0}$ is the low frequency diffusion length, $\omega_0 = \left(\tau^{-2} + 4\overline{G}\beta\right)^{1/2}$ is a characteristic recombination frequency, and $\tilde{\gamma}$ is a surface recombination factor as (S24.c) in the supplementary material.

Subsequently, the voltage and current responsivities can be deducted as

$$\Psi_V(\omega) = 2\frac{k_BT}{q\overline{G}}\frac{1}{\left(1+i\dfrac{\omega}{\omega_0}\right)}, \tag{10a}$$

$$\Psi_J(\omega) = \frac{q\overline{L}_d}{\sqrt{1+i\dfrac{\omega}{\omega_0}}}\tilde{\gamma}(1-\tilde{\delta}), \tag{10b}$$

with the complex diffusion length $\tilde{L}_d = \overline{L}_d(1+i\,\omega/\omega_0)^{1/2}$ and

$$\tilde{\delta} = S_r\frac{\left(e^{\frac{\overline{w}}{\tilde{L}_d}} - e^{\frac{L-\overline{w}}{\tilde{L}_d}}\right)}{\left(\dfrac{D}{\tilde{L}_d} + S_r + \left(\dfrac{D}{\tilde{L}_d} - S_r\right)e^{\frac{L}{\tilde{L}_d}}\right)}. \tag{10c}$$

Note that (10) shows how both functions behave with arc-shaped spectra since $\Psi_V \propto (1+i\,\omega/\omega_0)^{-1}$ and $\Psi_J \propto (1+i\,\omega/\omega_0)^{-1/2}$. Interestingly, (10) also suggests that at the low frequency limit, $\Psi_V \propto \overline{G}^{-1}$ but Ψ_J should be nearly $\overline{G}$-independent. Interestingly, if we weigh the predominant recombination term in ω_0 and apply the binomial series approximation, the low frequency limit from IMVS spectra can be used to straightforwardly evaluate the ideality factor m since

$$\Psi_V \cong m\frac{k_BT}{q\overline{G}}. \tag{10d}$$

In our simultaneous work,[8] we showed the agreement of (10d) with m obtained by IS and photocurrent-photovoltage curves of silicon, organic, and perovskite solar cells. However, while the IMPS low frequency limit (10b) seems to describe well the experiment for silicon solar cells, in the case of organic and perovskite solar cells, it fails, given that the p-i-n junction type is not in agreement with the hypothesis of depletion approximation and Eq. (5).

Subsequently, from (10a) and (10b), it is easy to obtain our LIMIS transfer function as

$$Z_\Psi(\omega) \cong \frac{2k_BT}{q^2\overline{L}_d\overline{G}}\frac{1}{\tilde{\gamma}\sqrt{1+i\dfrac{\omega}{\omega_0}(1-\tilde{\delta})}}. \tag{11}$$

Expression (11) for LIMIS is different from (9) for IS in only a factor, and so we can obtain the IS-LIMIS normalized impedance difference as

$$\Delta Z_\Psi = \frac{Z_\Psi - Z}{Z} = \frac{\tilde{\delta}}{1-\tilde{\delta}}, \tag{12}$$

which is directly proportional to S_r, as evident in (10c) and more explicitly in (S35) in the supplementary material, meaning that ΔZ_Ψ as (12) may inform on the surface recombination at the electrodes.

The model was used to simulate IS and LIMIS spectra from a p-n junction solar cell, whose full characterization can be found in our simultaneous work.[8] The experiments were performed with a Zennium Pro/PP211 impedance setup, from Zahner. The sample was a commercial 4 cm^2 silicon solar cell, also from Zahner, which facilitates the reproduction of our results. The cell was set under dc illumination intensity (Zahner LSW-2 white LED light source) until thermal equilibrium was reached, and sequentially, a small ac light perturbation was applied at the same frequencies for IMVS and IMPS measurements. For IMVS, the equipment sets the open-circuit (no absolute current is flowing) and the ac photovoltage signal is measured. For IMPS, the dc voltage corresponding to $\overline{V}_{oc}$ is applied (the absolute dc current is around nanoampere or lower), and the current signal at that bias due to the photocurrent modulation is measured. For IS, the measurement is idem to IMPS, except that the small perturbation is the ac voltage. Then, a series of dc illumination intensities are explored.

Figure 2 shows the experimental data and simulations in the Nyquist plot representation for the simulation parameters in Table S2 of the supplementary material. In all cases, the critical parameter defining the difference between both spectra was S_r, but further elements should be noted.

In a first example, Fig. 2(a) shows two spectra where IS and LIMIS are very similar; only the latter shows a slightly higher resistance. These patterns can be well simulated toward low frequencies by our model. The effect of reducing S_r is illustrated with dotted-dashed lines, indicating how LIMIS approaches IS, while ΔZ_Ψ is lessened. This is a "fingerprint" pattern for evaluating recombination velocity at the interfaces under moderate illumination rates, where $R_{LIMIS} \gtrsim R_{IS}$. Also, in Fig. 2(a), with dashed lines, we illustrate the role of increasing recombination via reducing the Shockley-Read-Hall lifetime τ of increasing the band-to-band recombination coefficient β. This results in the decrease in the impedances and the sign inversion of ΔZ_Ψ, meaning that IS may deliver more impedance than LIMIS, an already observed feature.[8] Here, the same value for extra series resistance R_s was added to the real parts of both impedances.

In Fig. 2(b), we highlight the resistances R_{IS} and R_{LIMIS} corresponding to the IS and LIMIS spectra, respectively. In this case, the situation is not so different from that observed in Fig. 2(a), with being R_{LIMIS} lightly higher than R_{IS}. However, differently, the LIMIS spectrum is significantly right shifted in what seems to be a series resistance effect at higher frequencies. The understanding of this feature is of particular difficulty due to the experimental limitations for measuring IMPS and IMVS and the reported more complex spectra shapes.[8] Also, it cannot be explained by our model, and so an extra term Z_s' was added to the $\mathrm{Re}[Z_\Psi(\omega)]$ in addition to the R_s, in common with the IS spectra.

Then, Fig. 2(c) displays the situation where R_{LIMIS} is no longer higher than R_{IS}, but still the Z_s' effect delivers a larger low frequency impedance from LIMIS with respect to IS. This situation better characterizes the case of higher illumination intensities. Remarkably, once more, S_r enhances the impedance difference between LIMIS and IS, as illustrated with the dotted-dashed lines in Fig. 2(c). Larger recombination velocity results in a higher absolute ΔZ_Ψ, most typically $\Delta Z_\Psi > 0$ at moderate or $\Delta Z_\Psi < 0$ under higher illumination intensities.

The above discussion reflects how our model may be complemented with further considerations in order to successfully reproduce the experiment. From our results, the ΔZ_Ψ parameter is first presented as a perspective figure of merit for the characterization of solar cells,

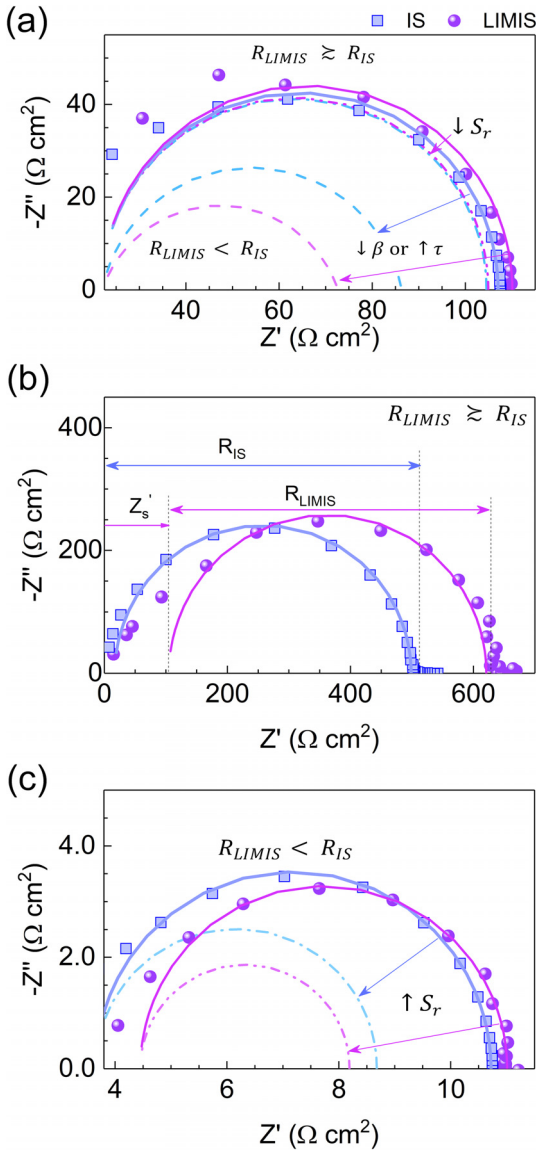

FIG. 2. Experimental spectra (dots) and our model simulations (lines) for IS, and LIMIS characterization of a standard p-n junction silicon solar cell at different illumination intensities $\overline{P}_{in}$. The effects when $S_r/5$ and $S_r \times 3$ are shown in (a) and (c), respectively. The measuring conditions and simulation parameters are summarized in Table S2 in the supplementary material.

here found to inform on S_r. However, future generalizations of this model may illustrate other parameters of interest from the experimental ΔZ_Ψ.

In summary, the time-dependent analytical solutions for the continuity equation considering diffusion currents in a one-sided p-n junction solar cell were found around the open-circuit steady-state upon small bias and light perturbations. This allowed us to show analytical expressions for the transfer functions of the potentiostatic impedance IS and the photoimpedance LIMIS. The difference between LIMIS and IS respective impedances resulted directly proportional to

the interface recombination velocity. The model was used to simulate experimental spectra from a silicon solar cell showing good agreement, mainly at lower frequencies. Extra experimental features as a series resistancelike right-shifting in the LIMIS Nyquist plots point out the limitations of the model toward high frequencies, suggesting the need for more realistic and numerical approaches.

See the supplementary material for the complete step-by-step deduction of the solutions of the transport equations and the simulation parameters.

We acknowledge the funding support from the Ministerio de-Ciencia, Innovación y Universidades of Spain under project (No. MAT2016-76892-C3-1-R). O.A. acknowledges the financial support from the VDI/VD Innovation + Technik GmbH (Project-title: PV-ZUM) and the SAOT funded by the German Research Foundation (DFG) in the framework of the German excellence initiative.

REFERENCES

[1]D. D. Macdonald, Electrochim. Acta **51**, 1376 (2006).
[2]J. Bisquert and F. Fabregat-Santiago, in *Dye-Sensitized Solar Cells*, edited by K. Kalyanasundaram (CRC Press, Lausanne, Switzerland, 2010), p. 457.
[3]O. Almora, K. T. Cho, S. Aghazada, I. Zimmermann, G. J. Matt, C. J. Brabec, M. K. Nazeeruddin, and G. Garcia-Belmonte, Nano Energy **48**, 63 (2018).
[4]O. Almora, L. G. Gerling, C. Voz, R. Alcubilla, J. Puigdollers, and G. Garcia-Belmonte, Sol. Energy Mater. Sol. Cells **168**, 221 (2017).
[5]O. Almora, C. Aranda, E. Mas-Marzá, and G. Garcia-Belmonte, Appl. Phys. Lett. **109**, 173903 (2016).
[6]O. Almora, M. García-Batlle, and G. Garcia-Belmonte, J. Phys. Chem. Lett. **10**, 3661 (2019).
[7]J. Bisquert, Phys. Chem. Chem. Phys. **5**, 5360 (2003).
[8]O. Almora, Y. Zhao, X. Du, T. Heumueller, G. J. Matt, G. Garcia-Belmonte, and C. J. Brabec, "Light intensity modulated impedance spectroscopy (LIMIS) in all-solid-state solar cells at open circuit," Nano Energy, e-print arXiv:1911.05440.
[9]O. Almora, C. Aranda, and G. Garcia-Belmonte, J. Phys. Chem. C **122**, 13450 (2018).
[10]Y. T. Set, E. Birgersson, and J. Luther, Phys. Rev. Appl. **5**, 054002 (2016).
[11]D. A. Jacobs, H. Shen, F. Pfeffer, J. Peng, T. P. White, F. J. Beck, and K. R. Catchpole, J. Appl. Phys. **124**, 225702 (2018).
[12]D. Moia, I. Gelmetti, P. Calado, W. Fisher, M. Stringer, O. Game, Y. Hu, P. Docampo, D. Lidzey, E. Palomares, J. Nelson, and P. R. F. Barnes, Energy Environ. Sci. **12**, 1296 (2019).
[13]J. A. Anta, J. Idígoras, E. Guillén, J. Villanueva-Cab, H. J. Mandujano-Ramírez, G. Oskam, L. Pellejà, and E. Palomares, Phys. Chem. Chem. Phys. **14**, 10285 (2012).
[14]E. Kamieniecki, J. Vac. Sci. Technol. **20**, 811 (1982).
[15]E. Kamieniecki, J. Appl. Phys. **54**, 6481 (1983).
[16]R. Peat and L. M. Peter, J. Electroanal. Chem. Interfacial Electrochem. **228**, 351 (1987).
[17]E. A. Ponomarev and L. M. Peter, J. Electroanal. Chem. **396**, 219 (1995).
[18]L. Dloczik, O. Ileperuma, I. Lauermann, L. M. Peter, E. A. Ponomarev, G. Redmond, N. J. Shaw, and I. Uhlendorf, J. Phys. Chem. B **101**, 10281 (1997).
[19]P. E. de Jongh and D. Vanmaekelbergh, J. Phys. Chem. B **101**, 2716 (1997).
[20]G.-O. Kim, Bull. Korean Chem. Soc. **33**, 469 (2012).
[21]A. Pockett, G. E. Eperon, T. Peltola, H. J. Snaith, A. Walker, L. M. Peter, and P. J. Cameron, J. Phys. Chem. C **119**, 3456 (2015).
[22]Y. Gao, A. J. Wise, A. K. Thomas, and J. K. Grey, ACS Appl. Mater. Interfaces **8**, 285 (2016).
[23]L. Bertoluzzi and J. Bisquert, J. Phys. Chem. Lett. **8**, 172 (2017).
[24]S. Ravishankar, C. Aranda, S. Sanchez, J. Bisquert, M. Saliba, and G. Garcia-Belmonte, J. Phys. Chem. C **123**, 6444 (2019).
[25]S. Ravishankar, A. Riquelme, S. K. Sarkar, M. Garcia-Batlle, G. Garcia-Belmonte, and J. Bisquert, J. Phys. Chem. C **123**, 24995 (2019).
[26]J. Krüger, R. Plass, M. Grätzel, P. J. Cameron, and L. M. Peter, J. Phys. Chem. B **107**, 7536 (2003).
[27]Y. T. Set, B. Li, F. J. Lim, E. Birgersson, and J. Luther, Appl. Phys. Lett. **107**, 173301 (2015).
[28]X. Chen, Y. Shirai, M. Yanagida, and K. Miyano, Phys. Chem. Chem. Phys. **20**, 17918 (2018).
[29]H. Song and D. D. Macdonald, J. Electrochem. Soc. **138**, 1408 (1991).
[30]J. Halme, Phys. Chem. Chem. Phys. **13**, 12435 (2011).
[31]J. Li and L. M. Peter, J. Electroanal. Chem. Interfacial Electrochem. **193**, 27 (1985).
[32]J. C. Byers, T. Heiser, M. Skorobogatiy, and O. A. Semenikhin, ACS Appl. Mater. Interfaces **8**, 28789 (2016).